High-Efficiency Power Supply for Resistive Loads with Sinusoidal Input Current

L. Rossetto*, L. Malesani*, G. Spiazzi**
J. A. Pomilio***, M. Monacchi****

**Department of Electrical Engineering, **Department of Electronics and Informatics*
University of Padova, Via Gradenigo 6/a, 35131 Padova - ITALY
Phone: +39-49-828.7500 Fax: +39-49-828.7599/7699
****Dept. de Sistemas e Controle de Energia*
UNICAMP, c.p. 6101, 13.081 Campinas - BRASIL
*****Whirlpool Europe*
Viale G. Borghi, 27, 21025 Comerio (Varese) - ITALY

***Abstract.* A high-quality rectifier for supplying resistive loads is presented. It features high power factor, low input current ripple and high efficiency. Device stresses are the same as for a buck converter, and input current is continuous.**

A suitable auxiliary network provides zero voltage switching for both power switch and diode.

The ripple steering technique was applied in order to reduce the input current ripple.

The converter, suitable for heating and lighting applications, was analyzed and experimentally tested on a 1kW prototype.

I. INTRODUCTION

The market for household appliances is becoming an important application area for power electronics. In fact, as compared to electromechanical devices, electronic power supplies offer superior performances at a similar cost. One of the main application area regards supplies for resistive loads in lighting and heating applications where futures like continuous power regulation, accuracy irrespective of line voltage variations, protection against short-circuits and open-circuits, power limitation etc. are becoming mandatory requirements.

On the other hand, electronic power supplies must be considered carefully as regards efficiency, reliability and harmonic distortion. From these points of view, topologies which provide low input current ripple are preferred, in order to reduce the size of the input filter. EMI problems are also crucial, calling for soft-switching techniques. Other common requirements for resistive loads are: direct supply from the utility line; high power factor; output power regulation from a few percent to 100% of rated power; high power density; limited power loss.

The care reserved to the utility line interface comes from the attempt to meet standard regulations and recommendations (like IEC 1000-3-2) while the severe environmental conditions, in terms of available space and ambient temperature, in which these power supplies can work call for high power density and efficiency.

In the following a simple high-quality rectifier for supplying resistive loads is presented and briefly analyzed in its several operating modes. The circuit features: high power factor, zero-voltage switching, obtained by using a suitable auxiliary network and low input current ripple, achieved by exploiting the ripple steering phenomenon.

Experimental results of a prototype are reported, showing actual converter performances.

II. BASIC CONVERTER SCHEME

The proposed converter scheme, shown in Fig. 1, is a step-down topology derived from the Cuk cell by a cyclic rotation of the components[1-3]. Due to the presence of the input inductor L_1, it draws a current with a much lower frequency content as compared to a standard buck converter. Moreover, this topology is suitable for the application of the ripple steering concept which further reduces the input current high-frequency ripple.

Due to the presence of two inductors and the diode bridge rectifier, more operation modes are possible. As reported in [3], besides the usual Continuous Conduction Mode (CCM) and Discontinuous Conduction Mode (DCM), the converter can work in Discontinuous Input Current Mode (DICM) in which only the input diodes stop conducting during the switch off-interval, and in Discontinuous Input and Output Current Mode (DIOCM), characterized by discontinuous currents in both inductors. Both these latter operation modes lead to different fundamental relations as compared to the buck converter; however, as suggested in [3], they are not recommended since produce a higher input current ripple and, above all, a higher switch voltage stress at light load, which limits the load range the converter can work with.

In the next section we will briefly review the converter behavior only for CCM and DCM operation modes; for a more comprehensive treatment the reader is suggested to consult [3].

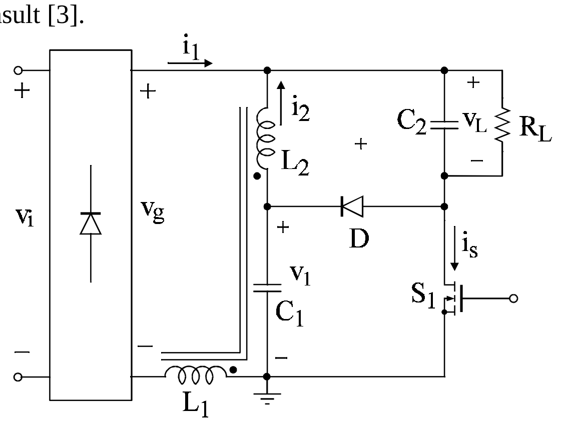

Fig.1 - Basic converter scheme

III. Review of Operation Modes: CCM and DCM

In the following analysis we will consider two separate inductors L_1 and L_2; the effects of the coupling will be taken into account later. For the application we are dealing with, the instantaneous output voltage, as well as the output power, is allowed to vary during the line cycle, since the goal is to control the average power supplied to the load. Thus, the circuit does not include large energy storage devices.

Assuming a switching frequency much higher than the line frequency, we can write:

$$v_g(\theta) = V_i \cdot |\sin(\theta)| \tag{1}$$

$$\bar{v}_L(\theta) = V_L \cdot |\sin(\theta)|, \qquad \theta = \omega_i t$$

where ω_i is the line angular frequency. Since all reactive elements of the converter are designed to handle energy at the switching frequency, from the power balance in a switching cycle, assuming unity converter efficiency, we can write:

$$v_g(\theta) \cdot \bar{i}_1(\theta) = \frac{\bar{v}_L^2(\theta)}{R_L} \quad \Rightarrow \quad \bar{i}_1(\theta) = \frac{M^2}{R_L} V_i |\sin(\theta)| \tag{2}$$

where the overbar means averaged quantities in a switching period and $M = \frac{\bar{v}_L(\theta)}{v_g(\theta)} = \frac{V_L}{V_i}$ is the voltage conversion ratio. This relation reveals that a high power factor is achieved for constant duty-cycle and switching frequency.

The relations and converter waveforms given hereafter are valid provided that the high-frequency voltage ripple across capacitors C_1 and C_2 is neglected.

1) CCM operation. Looking at Fig. 2a which reports the main converter waveforms during a switching period for the case of CCM operation, both inductor currents are continuous and the converter equations are the same of the buck topology. Both switch and freewheeling diode carry the sum of the two inductor currents during the on- and off-intervals respectively.

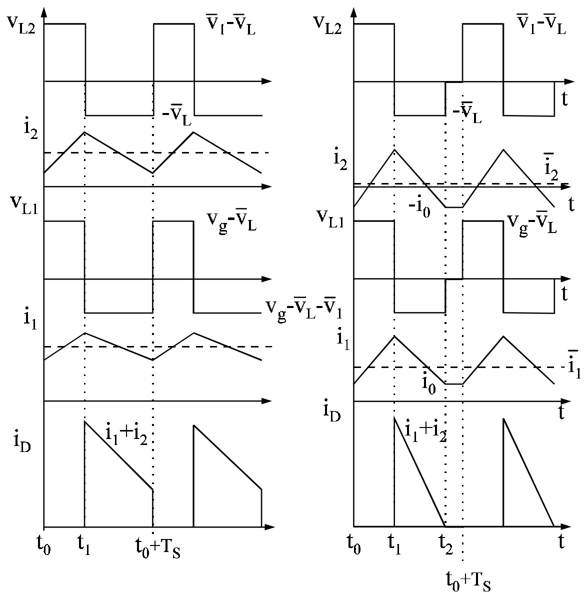

a) b)

Fig.2 - Main converter waveforms in a switching period. a) CCM operation, b) DCM operation

The volt-second balance applied to inductors L_1 and L_2 gives:

$$\bar{v}_1(\theta) = v_g(\theta)$$

$$M = \frac{\bar{v}_L(\theta)}{v_g(\theta)} = \frac{V_L}{V_i} = d \tag{3}$$

where d is the duty-cycle ($dT_S = t_0 \div t_1$). It is important to note that, due to the presence of the input diode bridge rectifier, current i_1 must always be greater than zero, leading to the following constraint on inductor L_1:

$$L_1 > \frac{R_L}{2 f_S} \cdot \left(\frac{1-M}{M} \right) \tag{4}$$

where f_S is the switching frequency.

From Fig. 2a it is also possible to calculate the peak current in both switch and freewheeling diode:

$$i_{S,peak} = i_{D,peak} = \frac{V_i}{R_L} \cdot M \cdot \left(1 + \frac{1-M}{k} \right)$$

$$k = \frac{2 L_e f_S}{R_L}, \qquad L_e = \frac{L_1 \cdot L_2}{L_1 + L_2} \tag{5}$$

1) DCM operation. With this operation mode the freewheeling diode current is discontinuous, leading to the typical waveforms of Fig. 2b. The main difference respect to the buck converter is that the input current remains continuous in spite of the zeroing of the diode current which, in fact, is the sum of the two's.

From the analysis of the waveforms of Fig. 2b we find that the first of (3) is still valid while the voltage conversion ratio results:

$$M = \frac{2}{1 + \sqrt{1 + \frac{4k}{d^2}}} \tag{6}$$

which is the same relation of a buck converter having an inductance equal to L_e.

Note that for the application we are dealing with, parameter k is constant because the load is assigned, while M must vary from zero to one in order to regulate the power delivered to the load. Thus, the value M_1 corresponding to the boundary between DCM and CCM operation is:

$$M_1 = 1 - k \tag{7}$$

The condition which ensures a current i_1 greater than zero is given by the inequality:

$$\frac{L_1}{L_2} > \frac{1-M}{M} \tag{8}$$

The switch and diode current stress is given by:

$$i_{S,peak} = i_{D,peak} = \frac{2V_i}{R_L} \cdot M \cdot \sqrt{\frac{1-M}{k}} \tag{9}$$

IV. Power Stage Design Criteria

As explained before it is convenient to design the converter for CCM and DCM operation modes only, in order to limit current and voltage stresses. While CCM operation, compared to DCM, ensures the lowest current ripples and thus the minimum current stresses and minimum conduction losses, it has the drawback of having higher turn on losses as well as EMI due to hard recovery of the freewheeling diode. Moreover, it requires high inductance values.

Taking into account the above considerations, it seems reasonable to design the converter in such a way that its operation mode changes from CCM to DCM when the voltage conversion ratio decreases from one to zero.

1) Converter Specification:

Peak Input voltage: .... V_i
Load Resistance:... R_L
Switching Frequency: .... f_S

2) Switch and Diode Current Stress. As stated above, at maximum output voltage (M = 1) the converter operates in CCM. Calling M_1 the value of the voltage conversion ratio in correspondence of which the converter enters the DCM region, the maximum normalized switch and diode current stress results (from (5) and (9)):

$$i_{SN,peak} = \frac{i_{S,peak} \cdot R_L}{V_i} = \begin{cases} \frac{4}{3\sqrt{3}} \frac{1}{\sqrt{k}} & \text{if} \quad k < \frac{1}{3} \\ \frac{(1+k)^2}{4k} & \text{if} \quad k > \frac{1}{3} \end{cases} \tag{10}$$

in which the relation k = 1-M_1 was used (see (7)).

Fig. 3 reports the variation of the normalized current stress as a function of parameter k. This plot can be useful to chose the value of k (and thus of M_1) making a trade off between the maximum allowed current stress, which calls for a high k value, and the inductor size, as it will result from the following analysis (in fact, high k means a wider range of CCM operation).

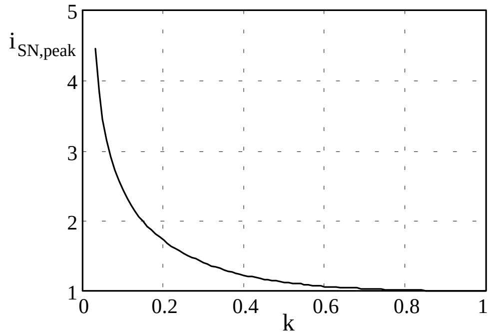

Fig. 3 - Normalized switch and diode current stress as a function of parameter k

3) Inductances L_1 and L_2. From (7) the value of parameter k is found as k = 1-M_1 and from its definition the value of equivalent inductance L_e is obtained as:

$$L_e = \frac{L_1 L_2}{L_1 + L_2} = \frac{R_L}{2 f_S} \cdot (1 - M_1) \tag{11}$$

A second constraint on the two inductors is given by inequality (8):

$$\frac{L_1}{L_2} > \frac{1-M_2}{M_2} \tag{12}$$

where M_2 is the value of the conversion ratio in correspondence of which current i_1 zeroes every switching cycle. This value must be chosen suitably lower than M_1, in order to reduce the input current ripple, thus reducing input filter requirements. From (11) and (12), the values of inductances L_1 and L_2 are derived as follows:

$$L_1 = \frac{R_L}{2 f_S} \cdot \left(\frac{1-M_1}{M_2} \right) \tag{13.a}$$

$$L_2 = \frac{R_L}{2 f_S} \cdot \left(\frac{1-M_1}{1-M_2} \right) \tag{13.b}$$

Note that the value of L_1 obtained from (13.a) automatically satisfies constraint (4) which, as demonstrated in [3], ensures a transfer from CCM to DCM operation without entering the DICM region.

4) Capacitance C_1 and C_2. The values of the two capacitances is chosen on the basis of the desired voltage ripples. For a detailed derivation of these ripples see reference [3].

V. Ripple Steering Concept

The ripple-steering phenomenon was originally investigated in Cuk converters [5], but it can effectively be applied to all converter topologies in which two or more inductors are fed by similar (scaled) voltage waveforms. And this is exactly the case for the proposed step-down topology (see Fig. 2a and 2b), since the first of (3) remains valid both for CCM and DCM operations. Thus we can draw the equivalent circuit model shown in Fig. 4.

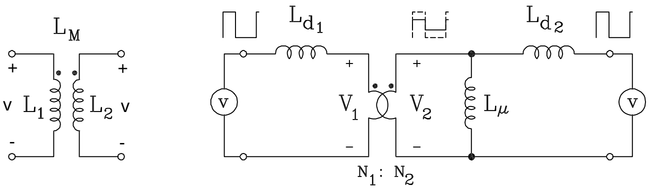

$$L_M = \frac{N_1}{N_2} \cdot L_\mu, \quad L_1 = L_{d1} + \left(\frac{N_1}{N_2}\right)^2 \cdot L_\mu, \quad L_2 = L_{d2} + L_\mu$$

Fig. 4 - Coupled-inductor equivalent circuit

As stated above, due to converter operation, the same voltage v is applied to both windings. Accordingly, zero ripple condition of primary current is easily derived by observing that secondary leakage inductance L_{d2} and magnetizing inductance L_μ form an inductive divider which scales the voltage applied to the secondary winding without altering its shape (voltage V_2 in Fig. 4). If turn ratio N_1/N_2 is chosen to step-up the voltage V_2 to the original value v, zero current ripple on the primary side is obtained. Thus, the zero ripple condition is [6]:

$$\frac{N_2}{N_1} = \frac{L_\mu}{L_\mu + L_{d2}} = k_r \tag{14}$$

where k_r is defined as secondary coupling coefficient. The input current ripple does not simply disappear, but it is "steered" into the other winding.

We can obtain the same result starting from the mutual inductor equations: assuming the same voltage applied on both windings, we can derive the rate of change of the currents in the two windings:

$$\frac{di_1}{dt} = \frac{v}{L_{1eq}}, \qquad \frac{di_2}{dt} = \frac{v}{L_{2eq}} \tag{15}$$

where,

$$L_{1eq} = L_1 \cdot \frac{1 - \frac{L_M^2}{L_1 L_2}}{1 - \frac{L_M}{L_2}}, \qquad L_{2eq} = L_2 \cdot \frac{1 - \frac{L_M^2}{L_1 L_2}}{1 - \frac{L_M}{L_1}} \tag{16}$$

From these expressions, it is seen that, to obtain zero ripple current in the input winding, the equivalent input inductance L_{1eq} must be infinity, which is accomplished by selecting $L_2 = L_M$. With this choice, we obtain also $L_{2eq} = L_2$. Using the relations reported in Fig. 4, it is easily verified that this zero ripple condition is equivalent to the previous one (14).

It is important to observe that the actual coupled inductor behavior deviates from the ideal one mainly for the following two reasons: the zero ripple condition (14) cannot be achieved due to integer number of turns and difficulty to set the gap thickness to the exact value required, and a real converter does not apply the same voltage to both inductor windings due to a non-zero voltage ripple on capacitors, DC voltage drop on inductors, switching noise and so on. As a consequence, the actual input current ripple depends also on the leakage inductance L_{d1} on the primary side.

As far as the design of the coupled inductors is concerned, there are three constraints that must be satisfied:

1) zero current ripple condition (14);
2) inductance L_2 must have the desired value imposed by the power stage design; in fact the equivalent inductance L_e as defined in (11), coincides with $L_{2eq} = L_2$ since L_{1eq} tends to infinity (see (16));
3) core saturation must be avoided.

For a detailed design procedure see [6].

VI. AUXILIARY CIRCUIT FOR SOFT-SWITCHING

In order to reduce the electromagnetic noise generated during commutations a suitable auxiliary circuit was used, which allows soft transitions for all switches and diodes. The auxiliary circuit, composed by components S_r, D_{r1}, D_{r2}, C_r and L_r, is shown in the equivalent scheme of Fig. 5 in which I_o corresponds to the sum of the two inductor currents i_1+i_2 and V_{in} represents the voltage across capacitor C_1 given by the first of (3). As described in [4], switch S_r is activated prior the main switch turn-on in order to discharge the parasitic capacitance of the main devices. In this way, the main switch turns on at zero voltage and, above all, a soft turn-off of the freewheeling diode is achieved, so avoiding the losses due to its recovery time.

Its behavior can be better understood by looking at the main converter waveforms reported in Fig. 6. Let us consider, initially, I_o and V_{in} constants. Before instant t_0, diode D is conducting the current I_o. At t_0 the auxiliary switch is turned on under zero current condition and the resonant current I_{Lr} rises linearly until it reaches the value I_o. Then, diode D is turned off in soft manner and L_r can resonate with parasitic capacitances C_d and C_s. At time t_2, the body diode of the main switch starts to conduct allowing the zero voltage turn on of S_1. When S_r is turned off (instant t_3), L_r resonates with C_r charging it to V_{in} through D_{r1}. Note that the auxiliary switch is turned off at zero voltage due to the presence of C_r. At instant t_4, D_{r2} starts conducting and I_{Lr} decreases linearly to zero flowing through S_1 and D_{r2}.

When S_1 is turned off its voltage increases linearly due to the charge of C_s and discharge of C_d and C_r until, at instant t_7 the diode D starts conducting initiating the usual freewheeling period. Note that all devices commutations are soft, both at turn on and turn off.

This is only one of the two possible operation modes in which we have assumed that, at instant t_3, the energy stored in L_r is able to completely charge C_r to V_{in}, i.e.:

$$\frac{1}{2} L_r \left(I_o + V_{in} \sqrt{\frac{C_{eq}}{L_r}} \right)^2 > \frac{1}{2} C_r V_{in}^2 \tag{17}$$

The other operation mode will be not considered here because it turns out to be less convenient then the first one. For more information see [4].

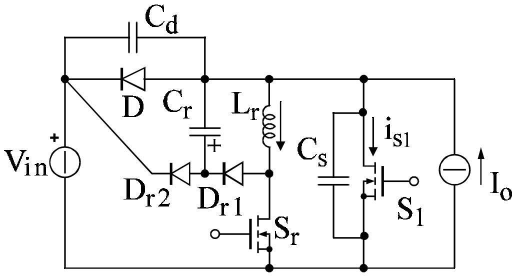

Fig 5 - Simplified schematics for analysis of the auxiliary circuit

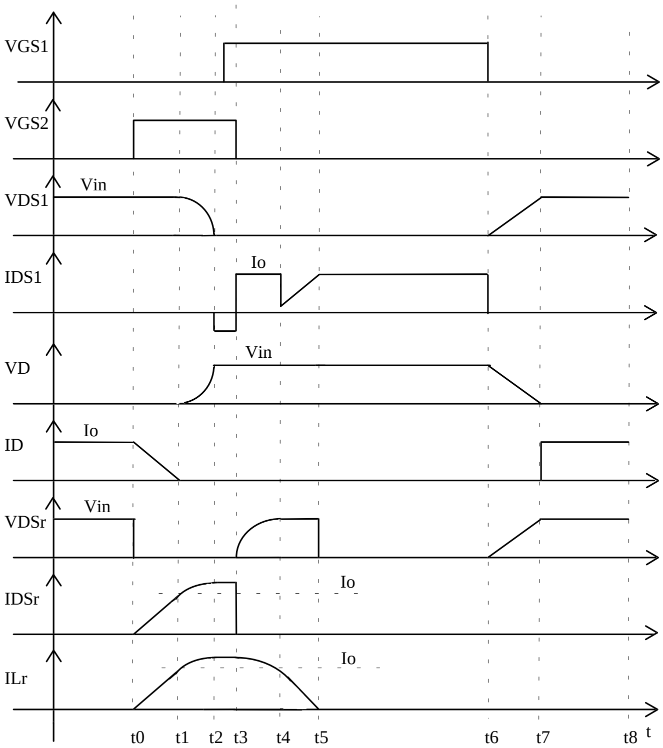

Fig. 6 - Main waveforms of the simplified circuit of Fig. 5b in a switching period

VII. AUXILIARY CIRCUIT DESIGN

The presence of the auxiliary circuit limits the available duty-cycle. In order to estimate these limits we define an effective off time as [4]:

$$t_{offe} = \frac{1}{V_{in}} \int_0^{T_s} v_{DS1} dt \tag{18}$$

Of course, such definition gives the usual off time in the case of hard switching converters in which v_{DS} is a square wave. According to (18), the equivalent duty-cycle is then given by:

$$\delta_e = \frac{t_{one}}{T_s} = \frac{T_s - t_{offe}}{T_s} \tag{19}$$

From the analysis of the waveforms of Fig. 6 the minimum value of the equivalent off time, which limits the maximum duty-cycle achievable, is:

$$t_{offe\,min} = \frac{I_o L_r}{V_{in}} + \sqrt{L_r C_{eq}} + \frac{V_{in}}{2I_o}\left(C_{eq} + C_r\right) \tag{20}$$

where $C_{eq} = C_d + C_s$. In the same manner the minimum switch on time can be derived as:

$$t_{one\,min} = \left(\frac{\pi}{2} - 1\right)\sqrt{L_r C_{eq}} + \frac{\pi}{2}\sqrt{L_r C_r} + \frac{V_{in}}{2I_o}\left(C_{eq} + C_r\right) \tag{21}$$

Now, we have to take into account that quantities I_o and V_{in} in the implementation of Fig. 1 are not constant. In particular, neglecting the high frequency voltage ripple across C_1, voltage V_{in} is equal to $v_g(\theta)$ while, I_o is equal to the load current $i_L(\theta)$ (the low frequency current in C_2 is negligible) given by:

$$\bar{i}_L(\theta) = \frac{\bar{v}_L(\theta)}{R_L} \tag{22}$$

Thus, since in (20) and (21) always compares the ratio between the two quantities we can write:

$$\frac{V_{in}}{I_o} = \frac{v_g(\theta)}{i_L(\theta)} = \frac{R_L}{M(\delta_e)} \tag{23}$$

Thus specifying the maximum and minimum duty-cycles from (3,17,19-22) the values of the auxiliary circuit parameters L_r, C_r and C_{eq} can be derived, and the current and voltage stresses of these components can be calculated [4]. It is worthy to note instead that current and voltage stresses of the main devices remain the same as the hard-switching solution.

Note that, in this application, the limitation on the maximum duty-cycle achievable does not cause particular problems. In fact, the maximum power transfer can be anyway achieved by keeping the main switch always closed and thus avoiding the commutation losses at maximum power.

VII. EXPERIMENTAL RESULTS

A prototype was designed and built with the following specifications: V_i = 220 V_{RMS}; P_L = 1 kW; f_s = 25 kHz.

The converter parameter values are listed in Table I in which the value of L_1 refers to the converter without magnetic coupling.

Fig. 10 shows the measured input current with and without magnetic coupling. The measurement was taken at a conversion ratio value which maximizes the current ripple: by comparison the magnetic coupling reduces the current ripple by a factor of six.

Table I - Converter parameters

L_1 = 400 µH	L_2 = 160 µH	C_1 = 2 µF	C_2 = 1 µF
C_r = 15 nF	L_r = 31 µH	C_{eq} = 7.5 nF	R_L = 48 Ω

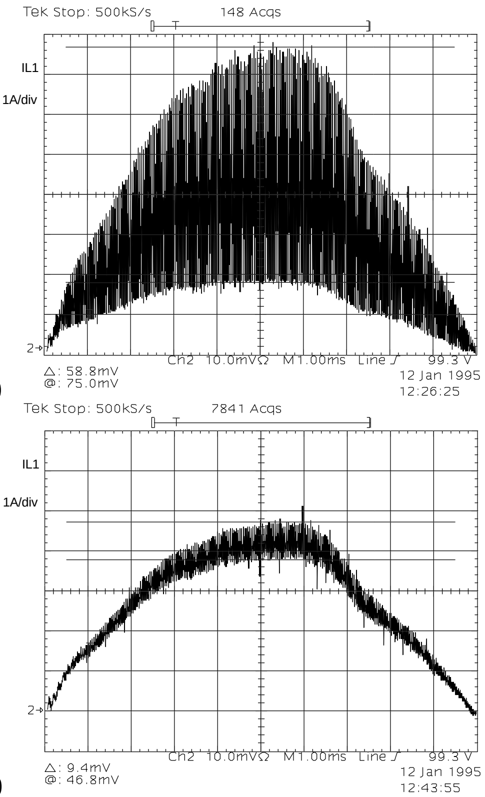

a)

b)

Fig. 10 - Input current waveform at V_i = 220V_{RMS} and I_i = 3A_{RMS}
a) without magnetic coupling; b) with magnetic coupling

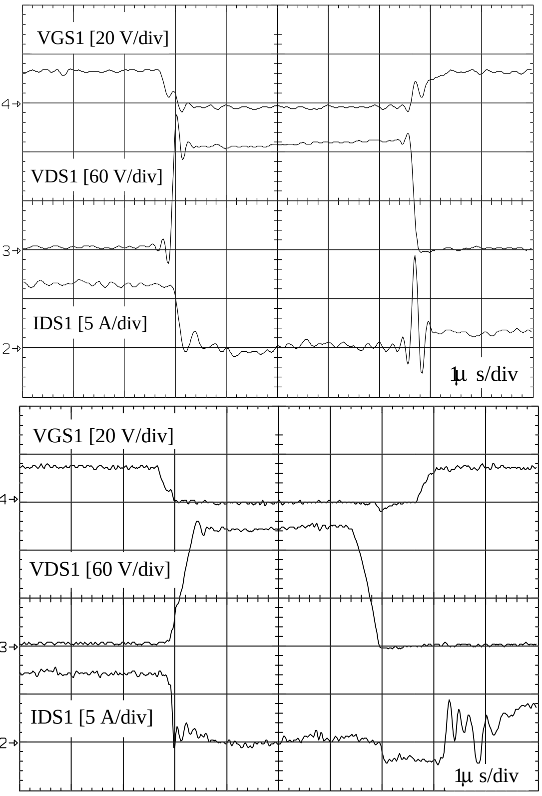

a)

b)

Fig. 11 - S_1 waveforms in a switching period.
a) without auxiliary circuit; b) with auxiliary circuit

The current total harmonic distortion is 5.8% while the line voltage distortion is 2.8%. The measured power factor is 0.998.

As far as the operation of the auxiliary circuit is concerned, Fig. 11 reports the comparison between the high frequency voltage and current waveforms of the main switch S_1 for the hard-switched and the soft-switched converter. The effects of the soft commutations are easily recognizable from Fig. 11b: at turn off the switch voltage stress is considerably reduced and, at turn on, no overlap between voltage and current occurs. Moreover, the big current spike due to the reverse recovery of diode D is eliminated.

The converter efficiency at the rated power remains approximately the same (about 95%) with and without the zero-voltage transition network. However the main advantage of the soft transitions is the reduced EMI.

VIII. Conclusions

A high-quality rectifier for supplying resistive loads, featuring continuous power regulation, high power factor, low input current distortion and high efficiency is presented. It has continuous input current and same device stresses of a standard buck converter.

A suitable auxiliary circuit was used which allows soft commutations for all devices .

Converter design criteria were given and experimental tests done on a 1kW prototype showed good agreement with the theoretical forecasts.

Acknowledgments

The authors would like to thank Dr. M. Miolo, whose dedicated work made possible experimental tests.

Thanks are also due to Mr. R. Sartorello, who supervised experimental activities.

References

[1] J. L. White, W. J. Muldoon, "Two-Inductor Boost and Buck Converters," IEEE Power Electronics Specialists' Conf. Rec., 1987, pp. 387-392.

[2] Z. Zhang, S. Cuk, "A High Efficiency 1.8 kW Battery Equalizer," IEEE Applied Power Electronic Conf. Proc., 1993, pp. 221-227.

[3] L. Rossetto, L. Malesani, G. Spiazzi, P. Tenti, J. A. Pomilio, C. Bocchiola, " High-Quality Rectifier for resistive Loads," Int. Conf. on Power Electronics, Drives and Energy Systems for Industrial Growth (PEDES), New dehli (India), January 1996, pp. 190-196.

[4] S. B. Yaakov, G. Ivensky, O. Levitin and A. Treiner, "Optimization of the Auxiliary Switch Components in a Flying Capacitor ZVS PWM Converters," Applied Power Electronics Conf. Proc., 1995, pp.503509.

[5] R.D.Middlebrook and S.Cuk, A*dvances in Switched-Mode Power Conversion*, vols. I and II, TESLAco, Pasadena, California, 1983.

[6] S.Cuk and Z.Zhang ,"Coupled-Inductor Analysis and Design", PESC Conf. Proc., 1986, pp. 655-665.